ACS APPLIED MATERIALS & INTERFACES

www.acsami.org Research Article

Recycling of Lignin and Si Waste for Advanced Si/C Battery Anodes

Weiwei Liu, Jing Liu, Menghua Zhu, Wenyu Wang, Lei Wang, Shangxian Xie,* Li Wang,* Xuelin Yang, Xiangming He, and Yongming Sun*

Cite This: https://dx.doi.org/10.1021/acsami.0c16865 Read Online

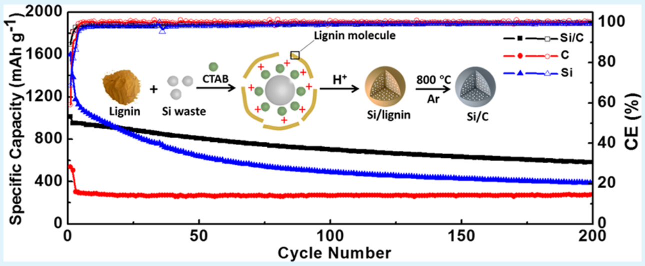

ABSTRACT: The ever-increasing silicon photovoltaics industry produces a huge annual production of silicon waste (2.03 × 10^5 tons in 2019), while lignin is one of the main waste materials in the traditional paper industry (7.0 × 10^7 tons annually), which lead to not only enormous wastage of resources but also serious environment pollution. Lithium-ion batteries (LIBs) are the dominating power sources for portable electronics and electric vehicles. Silicon (Si)-based material is the most promising anode choice for the next-generation high-energy-density LIBs due to its much higher capacity than the commercial graphite anode. Here, we proposed the use of these silicon and lignin waste as sustainable raw materials to fabricate high-capacity silicon/carbon (Si/C) anode materials for LIBs via a facile coprecipitation method utilizing electrostatic attracting force, followed by a thermal annealing process. The as-achieved Si/C composite featured an advanced material structure with micrometer-sized secondary particles and Si nanoparticles embedded in the carbon matrix, which could tackle the inherent challenges of Si materials, including low conductivity and large volume change during the lithiation/delithiation processes. As expected, the obtained Si/C composite displayed an initial charge capacity of 1016.8 mAh g^{-1}, which was 3 times that of a commercial graphite anode in the state-of-the-art LIBs, as well as a high capacity retention of 74.5% at 0.2 A g^{-1} after 100 cycles. In addition, this Si/C composite delivered superior rate capability with a high capacity of 575.9 mAh g^{-1} at 2 A g^{-1}, 63.4% of the capacity at 0.2 A g^{-1}. The utilization of industrial Si and lignin waste provides a sustainable route for the fabrication of advanced high-capacity anode materials for the next-generation LIBs with high economic and environmental feasibility.

KEYWORDS: *lithium-ion batteries, Si/C composite, solar Si waste, waste recycling, coprecipitation*

1. INTRODUCTION

Photovoltaics (PV) has played an important role in energy transition and grown at an unprecedented rate, which generates clean energy and can reduce 50% of the world's carbon emission and effectively suppress global warming.[1] Crystalline silicon PV is the dominating PV technology and shares 85−90% of the PV market.[2] Polycrystalline Si wafers are the basic materials for crystalline silicon PV, which are fabricated through multiwire slicing of Si ingots and has an annual output of 3.85 × 10^5 tons.[3] This process produces ∼40 wt % (∼1.54 × 10^5 tons) Si sawdust waste.[4] Figure 1 shows the production of polycrystalline Si ingot and the amount of Si waste from the perspective of time (Figure 1a), as well as their geographical distribution in the world (red text in Figure 1b) (data from China Photovoltaic Industry Alliance in 2020, URL of the web reference is listed).[54] The produced Si waste increased year by year accompanied by the product increase of polycrystalline Si ingots, and it reached a high value of 2.03 × 10^5 tons in 2019. China ranked number 1 for both the products of polycrystalline Si ingots and Si waste according to their geographical distribution in 2019. Five countries, including China, Korea, Germany, the United States, and Japan, shared 97.7% of the global products. The produced huge amount of Si waste and its accumulation from the Si PV industry cause ever-increasing environmental pollution and waste of resources.[5] Thus, it is highly desirable to explore an economical and environmentally friendly approach to recycle the Si waste from the PV industry.

Biomaterials as a natural carbon source have been widely utilized to organize nanostructures with special features.[6−8] Lignin, as one of the most abundant biomass resources on the earth, is generated on a large scale as a low-value waste product from the pulp and paper industry and biorefinery. However, owing to the random structure heterogeneity of lignin connected by several types of covalent bonds described as "chemical web", it is highly recalcitrant to biological degradation and thus discharged along with the pulp wastewater, which has caused serious environmental prob-

Received: September 18, 2020
Accepted: November 26, 2020

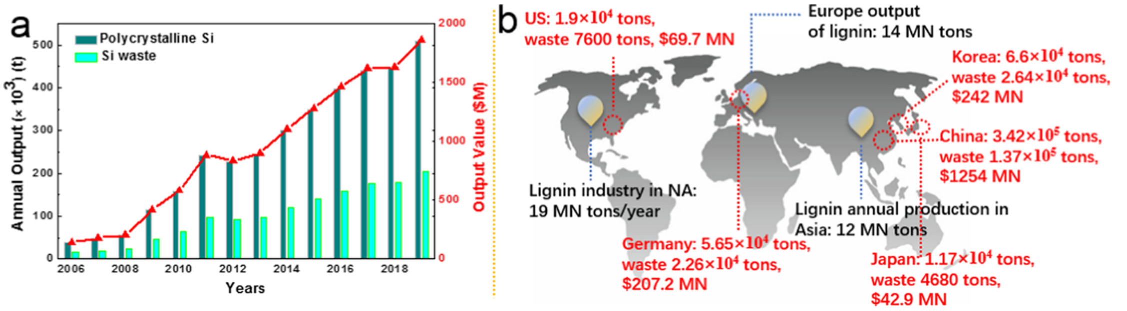

Figure 1. (a) Annual production of polycrystalline Si and Si waste (~40 wt % of the polycrystalline Si) in recent years and the corresponding estimated value (calculated based on the capacity of Si/C and graphite). (b) Global distribution of polycrystalline Si (in red text) and its estimated value and lignin output distribution in 2019 (in black text).

lems.[9,10] Currently, it has a worldwide production of 7.0×10^7 tons annually from the pulp industry with a commercial value of only USD 732.7 million, while it is expected to reach 22.5×10^7 tons by 2030 with an estimated annual growth rate of 12% (Figure 1b).[11,12] Additionally, the development of next generation of biorefinery will produce an even much higher amount of lignin waste. Thus, to create an application of lignin to a valuable product with compatible market scales to the annually produced lignin can not only effectively reduce environmental pollution but also achieve considerable economic benefits.

Coupled with energy transmission (e.g., PV), energy storage plays a crucial role in the landscape of energy processes. As one of the most successful commercially available energy storage technologies, lithium-ion batteries (LIBs) using a graphite anode and a transition-metal oxide cathode are dominating consumer electronics and electric vehicles.[13,14] To meet the increasing energy demand of LIBs for advanced applications, it is of vital importance to further increase the energy and power density of LIBs using new battery chemistry based on different lithium storage mechanisms. For example, an alloy reaction-type Si material delivers 10 times higher theoretical capacity (4200 mAh g^{-1} based on $Li_{4.4}Si$) than the intercalation-type graphite material (372 mAh g^{-1} based on LiC_6).[15,16] Much improved energy density of LIBs can be expected if the graphite anode is replaced by a Si-based anode, which represents the most promising approach to improve current LIBs for short-term purposes.[17−19] If calculated based on the capacity (372 mAh g^{-1}) and production value of the commercial graphite anode (400 thousand tons equals $1.1 billion), the output value of the anode based on the Si waste could reach $1.86 billion in 2019. The global distribution of this output is shown in Figure 1b, where the values from Germany and China would be $207.2 million and $1254 million, respectively.

However, Si suffers from poor electronic conductivity (~10^{-3} S cm^{-1}), huge volume variation of Si (>300%) during (de)alloying with lithium, and the as-resulting unstable solid electrolyte interphase (SEI), which lead to considerable lithium loss and consumption of a liquid electrolyte over cycling and thereby degrade the electrochemical performance.[20−23] To overcome the aforementioned problems and achieve high-performance Si anodes, various strategies have been explored, including electrolyte engineering, nanostructure configuration, and Si/graphite composite.[24−26] Among them, the construction of the Si/C composite using carbonaceous materials as a buffer matrix for Si particles has been demonstrated as a viable route to realize the good electrochemical performance of the Si-based anode.[27,28]

Here, we proposed to fabricate the high-performance Si/C composite anode material for advanced LIBs using the Si waste from the PV industry as the active material and lignin waste as the carbon source, which can not only address the environmental problem caused by these two waste materials but also bring huge economic benefits. Using lignin and solar Si waste as raw material, large-scale production of Si particles encapsulated in lignin-based amorphous carbon (denoted Si/C) has been realized through the facile coprecipitation process in ambient conditions, followed by thermal annealing at 800 °C. Owing to the abundant −OH functional groups on lignin molecules, the lignin solution presents electronegative. During the fabrication, the coprecipitation process is enabled by electrostatic attraction between cationic surfactant cetyltrimethyl ammonium bromide (CTAB)-modified Si particles and electronegative lignin molecules. Uniform Si/C composites, featuring Si particles with a size of 150−300 nm uniformly embedded in a carbon matrix, was synthesized after carbonization of the lignin. The carbon matrix can effectively alleviate the stress from the volume variation of Si during the lithiation and delithiation processes and reduce the amount of SEI by decreasing the direct contact between active Si and the electrolyte. As expected, the as-achieved Si/C composite showed a high overall charge capacity of 706.8 mAh g^{-1} at 0.2 A g^{-1} after 100 cycles, which doubles the capacity of the existing graphite anode. Also, the specific Si/C composite exhibited high rate capability, which delivered capacities of 907.9 and 575.9 mAh g^{-1} at 0.2 and 2 A g^{-1}, respectively. Such advanced Si/C anode material demonstrates great potential in commercial applications for next-generation LIBs. Meanwhile, the efficient recovery of lignin and Si waste makes a great contribution to solving environmental pollution and save natural resources.

2. EXPERIMENTAL SECTION

2.1. Material Preparation. Solar waste silicon powder was received from Golden Concord Holdings Limited Co. and used after mechanically ball milling for 20 h at 350 r/min and washing with a 10 wt % HF solution and DI water. Silicon powder (40 mg) was dispersed in 40 mL of deionized water containing 90 mg of CTAB. The suspension was sonicated and stirred for 30 min. The lignin used in this study was prepared from the soda pulping black liquor following the protocol as described in our previous study.[29] The purified lignin powder (400 mg) was dissolved in 40 mL of KOH solution (60 mmol L^{-1}) under strong stirring. After the lignin solution became brown, the silicon dispersion was dripped into the lignin solution under vigorous stirring to obtain a homogeneous suspension.

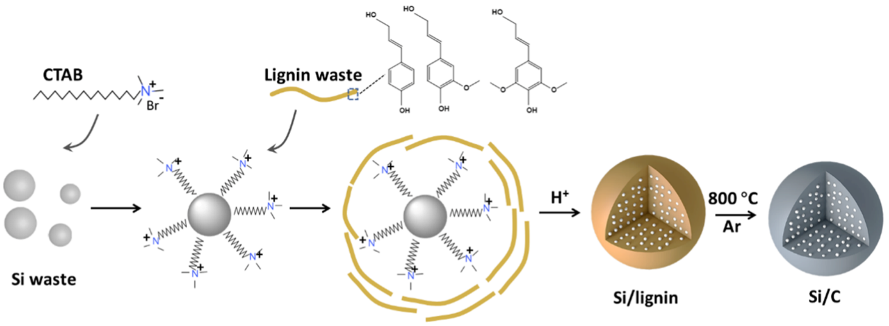

Figure 2. Schematic illustration of the preparation of the Si/C composite.

Subsequently, 500 μL of sulfuric acid (2 mol L^{-1}) was added and the Si/lignin precursor precipitated out. The resulting Si/lignin composites were collected by centrifugation and washed with deionized water three times and dried at 60 °C in a vacuum oven overnight. Finally, Si/C composite materials were obtained after annealing at 800 °C for 2 h with a ramping rate of 5 °C min^{-1} under an Ar atmosphere.

2.2. Material Characterization. The morphology and microstructure were characterized by field-emission scanning electron microscopy (FESEM, Nova NanoSEM 450) and transmission electron microscopy (TEM, Talos F200X), respectively. The crystallographic information and phase purity of the samples were investigated by X-ray diffraction (XRD, Empyrean) with Cu Kα radiation and Raman spectroscopy (LabRAM HR800). Fourier transform infrared (FTIR, Vertex 70) spectroscopy and X-ray photoelectron spectroscopy (XPS, AXIS-ULTRA DLD-600W) with a monochromatic Al Kα X-ray source were employed to analyze the chemical composition. Thermogravimetric analysis (TGA) was conducted with a ramping rate of 5 °C min^{-1} at ambient conditions on a TA-Q50 instrument.

2.3. Electrochemical Measurements. Si/C electrodes were fabricated by a slurry approach that was cast on copper foil using a blade and then dried in vacuum at 60 °C for 12 h. The electrode comprised 80 wt % active materials (Si/C composite), 10 wt % conductive additive (super P), and 10 wt % binder (poly(acrylic acid)). The mass loading of electrodes was ~1.3 mg cm^{-2}. All of the electrochemical measurements were performed using CR2032-type coin cells. A Celgard 2500 membrane was used as the separator, and Li metallic foil was used as the counter electrode. The electrolyte was 1.0 M $LiPF_6$ in a mixture of ethylene carbonate and diethylcarbonate (1:1 by volume) with 5 wt % fluoroethylene carbonate (FEC) as the additive. The cells were assembled in an argon-filled glovebox with O_2 and H_2O both <0.1 ppm. The galvanostatic discharge/charge (GDC) measurements of the cells were carried out at 25 °C in a voltage range of 0.01−2.0 V versus Li/Li^+ on a Neware multichannel battery testing instrument. The specific capacities were calculated based on the mass of the active materials (Si/C composite). The cyclic voltammetry (CV) and electrochemical impedance spectroscopy (EIS) measurements were conducted on a VMP3 multichannel potentiostat (Bio-Logic). The impedance performance was tested under open circuit potential with an amplitude of 10 mV at a frequency range of 100 kHz to 0.01 Hz.

3. RESULTS AND DISCUSSION

The two-step synthesis process of Si/C composites is shown in Figure 2. The fabrication of the Si/lignin precursor is implemented through coprecipitation of lignin molecules and Si particles under electrostatic attracting force. As evidenced by FTIR spectra, abundant −OH functional groups exist in lignin (Figure 4a), making it electronegative. To realize the electrostatic attraction between lignin and Si, cationic surfactant CTAB is added to the Si particle suspension to perform Si surface cationization. When the two solutions/suspensions undergo strong stirring, the Si particles are surrounded by lignocellulose due to the electrostatic attraction. Then, the coprecipitation process is triggered by dipping a bit of H^+ into the mixed liquor. Because the H^+ is incompatible with −OH functional groups on lignin, the lignin is precipitated from the mixture with the Si particles embedded in under electrostatic attraction. Finally, after annealing of the Si/lignin composite at 800 °C under Ar, the Si/C composite is obtained.

The morphology and microstructure of the as-obtained products are characterized by SEM and TEM. Figure 3a shows the changes of samples during the fabrication process of the Si/lignin composite. The lignin solution is a brown solution (Figure 3a, left). The Si/lignin composite is coprecipitated out from the mixture solution of Si/CTAB and lignin after adding H^+, which makes the color of the supernatant change from brown to nearly colorless, indicating that the lignin molecules have precipitated out from the solution (Figure 3a, middle and right). Figure 3b shows the SEM image of the solar Si waste with sizes ranging from 150 to 300 nm. The SEM results of the lignin waste powder show a random block without fixed size from a hundred nanometers to several micrometers (Figure 3c). Figure 3d,e shows the SEM images of the Si/C composite.

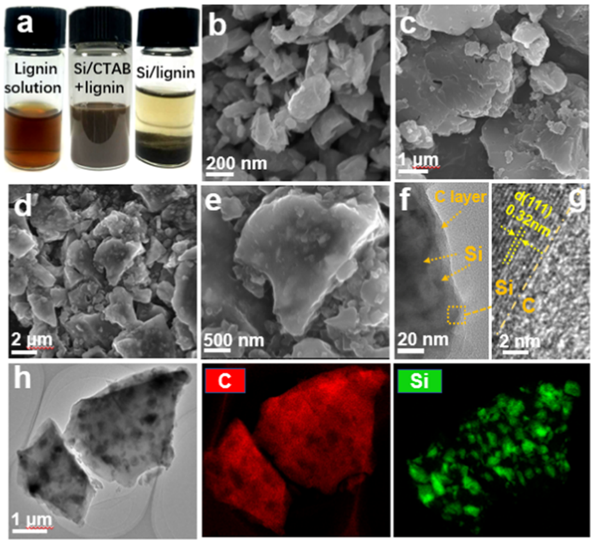

Figure 3. (a) Optical images of the materials fabrication process. (b) SEM image of the Si powder. (c) SEM image of the lignin powder. (d, e) SEM images of the Si/C composite. (f, g) TEM and HR-TEM image of the Si/C composite. (h) STEM image of the Si/C composite and the corresponding elemental mapping images of C and Si.

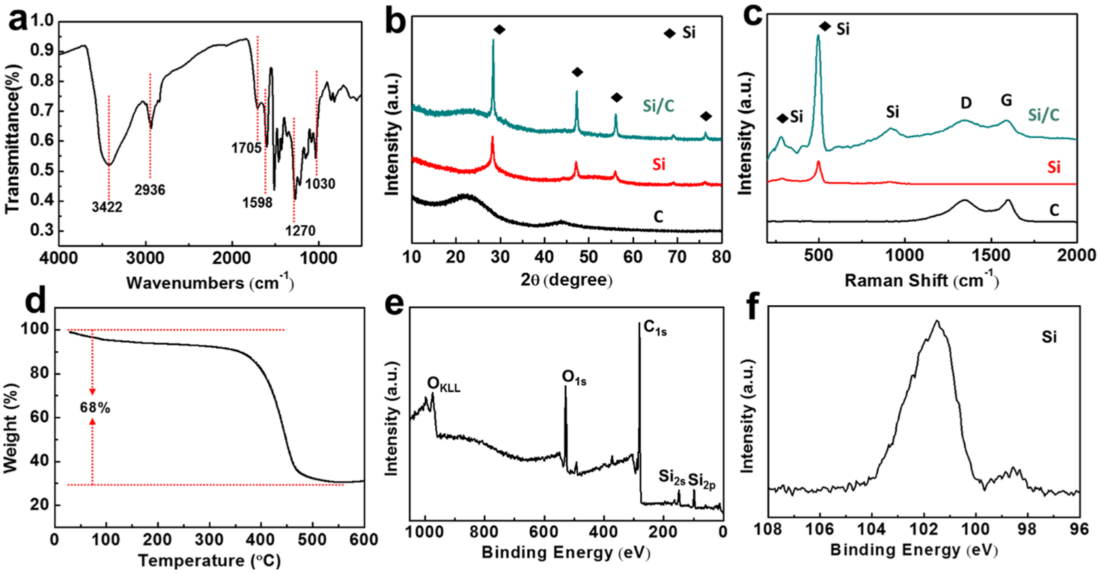

Figure 4. (a) FT-IR spectrum of the lignin powder. (b) XRD patterns and (c) Raman spectra of the Si/C composite, pure Si, and lignin-based C. (d) TGA of the Si/C composite. (e) XPS survey spectrum and (f) high-resolution Si 2p spectrum of the Si/C composite.

Irregular particles with a size of several micrometers are observed, which can reduce the exposed area of Si and suppress the undesirable reactions between active Si and the electrolyte. From the TEM image of Si/C in Figure 3f, it can be found that Si is embedded in a matrix of amorphous carbon. A clear lattice fringe with a 0.32 nm spacing, which corresponds to the (111) lattice plane of Si is observed in the high-resolution TEM image (Figure 3g), as well as the carbon layer on the Si particles. To verify the important role of CTAB in the formation of a uniform structure of the Si/lignin (Si/C) composite, the Si−C composite is fabricated by the same experimental procedure without the addition of CTAB. Figure S1a shows the electron microscopy characterization of the Si−C composite. It is observed that the agglomerated Si particles are located on the surface of carbon and the distribution of Si in the composite is inhomogeneous. Because of no electrostatic attraction between lignin and bare Si without modification of CTAB, the precipitation of Si/lignin is not uniform. The irregular structure of the as-achieved Si−C is further confirmed by TEM investigation (Figure S1b). Some Si particles are completely exposed outside the carbon. Such a simple physical blend feature of the Si−C composite will lead to the failure of carbon protection and rapid capacity decay in long-term discharge/charge cycling.

Scanning TEM (STEM) images of the Si/C composite and the corresponding element energy-dispersive spectroscopy (EDS) mapping images for C and Si elements are shown in Figure 3h. The result indicates that the dark particles corresponding to the Si particles that are embedded homogeneously within the gray area (the carbon matrix) result in an enhanced electrical conductivity and improved accessibility and diffusivity of Li^+ ions.[28] Also, the carbon matrix helps to buffer the volume change during the lithiation/delithiation of Si and thus enhances the cycling stability of the electrode. More importantly, the carbon matrix can protect the Si particles from direct contact with the electrolyte and relieve the stress from the volume variation of Si during the lithiation process by which both can promote stable electrochemical performance.[30]

FT-IR is employed to examine the chemical functional groups of lignin (Figure 4a). The absorption band at 3422 cm^{-1} is assigned to the O−H stretching vibration of hydroxyl groups, which is attributed to aliphatic and phenolic structures.[31,32] Owing to these O−H groups, lignin can be easily dissolved in an alkaline solution and precipitated in an acid environment. The marked absorption bands at 2936, 1705, and 1598 cm^{-1} correspond to the C−H bond of methyl and methylene groups, carbonyl groups, and aromatic-ring vibration, respectively, which constitute the basic structure of lignin. The bands at 1270 and 1030 cm^{-1} are ascribed to C−O stretching. All of these abundant organic functional groups determine the solubility in different pH values, which is important for the fabrication of Si/lignin composites. The crystallinity and phase purity of the as-prepared Si/C composite, lignin-based C, and bare Si are characterized by XRD measurements. As shown in Figure 4b, all of the sharp diffraction peaks at 2θ values of 28.5, 47.5, 56, and 76.2° correspond to (110), (220), (311), and (331) planes of Si (JCPDS no. 27-1402), respectively. Apart from the wide peak at around 23° for amorphous carbon, no other diffraction peaks are observed, suggesting the phase information of crystalline Si and amorphous carbon. Raman spectra are used to study the chemical structure of the as-obtained product (Figure 4c). The weak peak at 285 cm^{-1} of Si/C is ascribed to the second acoustic phonon mode of Si, while the strong peak centered at 501 cm^{-1} is characteristic of the first scattering from optic phonons of the Si−Si stretching mode in crystalline Si.[33,34] Additionally, the two broad peaks located at about 1343 and 1595 cm^{-1} correspond to the D and G bands of the carbon matrix, respectively.[35]

TGA is tested under air at a heating rate of 5 °C min^{-1} to analyze the content of Si in the Si/C composite. As shown in Figure 4d, the weight keeps decreasing as the temperature increases to ∼550 °C owing to the oxidation of amorphous carbon. The residual is Si after the removal of carbon and the content of Si is nearly 30% according to the TGA result. The surface element component of the Si/C composite is investigated by the XPS measurement. The survey spectra show typical peaks for Si, C, and O elements, indicating the

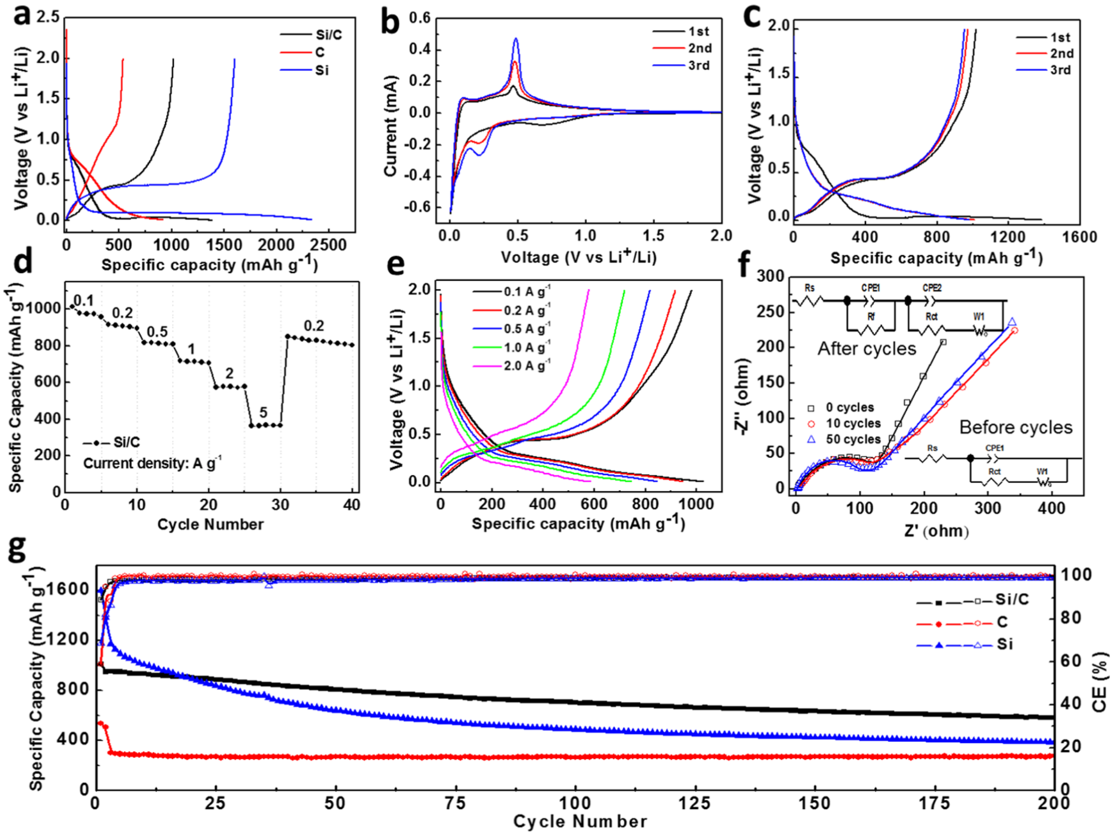

Figure 5. (a) First discharge−charge curves of the Si/C composite, pure Si, and C at 0.1 A g^{-1}. (b) CV curves of the Si/C electrode for the first three cycles at a scan rate of 0.1 mV s^{-1}. (c) Discharge−charge curves of the Si/C electrode for the first three cycles at 0.1 A g^{-1}. (d) Rate capability and (e) GDC curves of the Si/C electrode at different current densities. (f) Nyquist plots of the Si/C electrode at different cycles. (g) Capacity−cycle number plot and CE−cycle number plot of the Si/C, pure Si, and C anodes at 0.2 A g^{-1}.

elemental composition of the Si/C composite (Figure 4e).[36] Figure 4f shows the high-resolution Si_{2p} spectrum. Two peaks at ∼101.5 and ∼98.5 eV are observed. The latter arises from Si^0, while the former corresponds to Si^{2+}, suggesting the partial oxidation of Si particles.[18] The aforementioned results, including XRD, SEM, TEM, and EDS, indicate that the Si/C composite featured by Si nanoparticles encapsulated in a lignin-derived carbon matrix is successfully synthesized through a facile solution coprecipitation process followed by thermal annealing.

The electrochemical lithium storage properties of the samples are investigated using a coin-type half-cell configuration. The specific capacities are calculated based on the total mass loading of the Si/C composite materials. Figure 5a shows the initial galvanostatic discharge−charge (GDC) curves of the pure Si, C, and Si/C composite at 0.1 A g^{-1} within the potential range of 0.01−2 V. The discharge/charge capacities are 2333.8/1602.4, 912.6/538.4, and 1384.4/1016.8 mAh g^{-1}, respectively. The corresponding initial charge−discharge efficiencies (ICEs) of Si, C, and Si/C are 68.7, 59.0, and 73.4%, respectively. Compared to the pure Si and lignin-based C, the increased ICE value of the Si/C composite is attributed to the reduced surface area of the composite structure, which can reduce the exposed area of active materials to the electrolyte and the undesirable side reactions between them.[37] Amorphous carbon often leads to large irreversible capacity and low initial Coulombic efficiency for battery anode materials.[38,39] For the as-fabricated Si/C composite, the high content of carbon and its amorphous structure cause the large first irreversible capacity. Figure 5b shows cyclic voltammetry (CV) curves of the Si/C composite for the first three cycles with a scan rate of 0.1 mV s^{-1}. On the first cathodic scan curve, a broad peak within the range of 0.4−1.0 V is ascribed to the decomposition of the electrolyte and the formation of SEI.[40,41] In the subsequent cycles, this broad peak disappears, indicating that a stable SEI film is formed after the initial lithiation process. The cathodic peak at around 0.2 V for the second cycle is attributed to the alloying process to form metastable amorphous Li_xSi.[42] In the anodic sweep section, the peak at 0.5 V corresponds to the dealloying reaction from Li_xSi to Si. Within the first three cycles, the intensity of the anodic and cathodic peaks gradually increases, demonstrating the electrochemical activation process of the Si/C electrode.[43]

Figure 5c shows the first three GDC profiles of the Si/C electrode at a current density of 0.1 A g^{-1}. During the initial lithiation process, a potential slope from 0.8 to 0.1 V can be attributed to the decomposition of the electrolyte and the formation of SEI.[44] The flat and long voltage platform results from the transformation from crystalline Si to amorphous Li_xSi. The initial discharge and charge capacities are 1384.4 and 1016.8 mAh g^{-1}, leading to an ICE value of 73.4%. The capacity loss is mainly ascribed to the inevitable formation of SEI and irreversible reaction between active lithium and the oxygen-containing functional groups on the carbon matrix surface.[45] The CE value fast reaches nearly 100% during the second and third cycles, suggesting the stable surface structure due to the formation of SEI during the initial cycle. In the following cycles, couples of potential plateaus at 0.45 V on

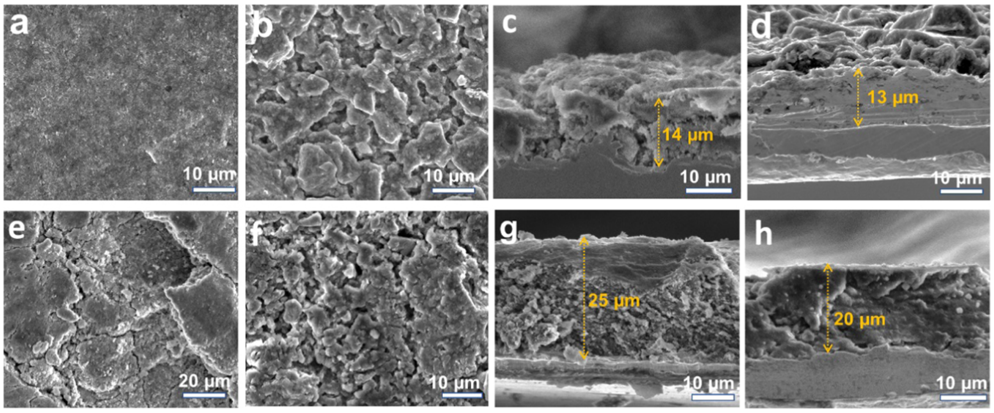

Figure 6. (a, e) Morphology changes of the pure Si electrode and (b, f) Si/C electrode before and after 100 cycles. (c, g) Cross-sectional SEM images of the pure Si electrode and (d, h) Si/C electrode before and after 100 cycles.

average on the charge curves and 0.25 V on average on the discharge curves correspond to the dealloying and alloying reactions of Si. These GDC results are in good agreement with the CV curves in Figure 5b.

To evaluate the rate capability of the Si/C electrode, GDC measurements have been performed at different current densities from 0.1 to 5 A g^{-1}, followed by a recovered current density of 0.2 A g^{-1} (Figure 5d). It is clearly observed that the specific capacity gradually decreases along with the increased current density and it recovers to the previous value when reverted back to 0.2 A g^{-1}. The specific capacities are 980.8, 907.9, 813.4, 712.9, and 575.9 mAh g^{-1} at current densities of 0.1, 0.2, 0.5, 1, and 2 A g^{-1}, respectively, suggesting the good rate capacity of the Si/C electrode. When the current density returns to 0.2 A g^{-1}, the Si/C electrode displays a capacity of 826.4 mAh g^{-1}, close to the value initially measured at the same current density, indicating superior stability of the Si/C electrode. The fast reaction kinetics is correlated with the advanced structure of the Si/C composite featured with Si particles embedded in the lignin-based carbon matrix, which ensures rapid mobility of electrons and ions.[46] Figure 5e shows the corresponding GDC curves at different current densities. There is no obvious change in the average potential for the Si/C electrode tested at different current densities, and the difference in electrochemical polarization from 0.1 to 2.0 A g^{-1} is as small as 0.05V, which benefits from the fast electron/ion-transport capability of the as-achieved material.[47] The good conductivity and fast electrochemical reaction kinetics of the Si/C electrode have also been verified by the EIS result. As shown in Figure 5f, the fitted Nyquist plots based on the corresponding equivalent circuits diagram exhibit a semicircle in the high-frequency region and a slope low frequency line, which represent the charge-transfer resistance (R_{ct}) on the electrode/electrolyte interface and diffusion resistance of Li ions in the electrode,[40,48] respectively. Before cycling, the pure Si electrode exhibits a much higher R_{ct} impedance of 166.2 Ω. This value decreases to 120.7 Ω for the Si/C electrode (Figure S2). After ten cycles, the semicircles size of the Si/C electrode becomes smaller than that before cycling, indicating decreased resistance, which may be ascribed to the activation process of the electrode.[49] Moreover, the Nyquist plots for the 10 and 50 cycles overlap well with R_{ct} values of 111.5 and 109.5 Ω, respectively, indicating the good stability of the Si/C electrode benefited from the advanced material structure where Si initial particles are encapsulated in a lignin-based carbon matrix.

The long-term cycling stability of the Si/C electrode has been evaluated by GDC measurements at a current density of 0.2 A g^{-1} (Figure 5g). After activation at 0.1 A g^{-1} for the first three cycles, the Si/C electrode displays a charge capacity of 949.6 mAh g^{-1} for the first cycle at 0.2 A g^{-1} and 706.8 mAh g^{-1} after 100 cycles, which doubles the capacity of the state-of-the-art graphite electrode in LIBs. When the cycle numbers extended to 200, a reasonably high specific capacity of 584.1 mAh g^{-1} was still achieved. In comparison, the pure Si anode presents a much lower specific capacity of 389.0 mAh g^{-1} at the 200th cycle, which is mainly caused by the deterioration of active Si and the loss of the electrical contact.[50] The lignin-based carbon anode shows stable cycle stability but delivers a low charge capacity of 277.6 mAh g^{-1} over 200 cycles. Our lignin-based Si/C anode presents a competitive battery performance in comparison to Si/C composites using other biomass as carbon sources such as corn starch, bamboo charcoal, sucrose, and reed leaves.[13,51−53] Consequently, the Si/C composite prepared by the facile coprecipitation method using the Si waste exhibits obvious performance advantages over pure Si and lignin-based carbon anodes. The improved electrochemical performance is mainly correlated with the carbon matrix, which can prevent Si particles from direct contact with the electrolyte as well as alleviating the stress from the volume change of Si. Importantly, such a Si/C electrode with superior electrochemical performance is prepared with cheap raw materials and by a facile fabrication process, which provides a sustainable route to the commercial application of Si waste as a high-performance battery anode.

The structure and morphology changes of electrodes before and after cycling have been examined by SEM (Figure 6). The electrodes for thickness measurements are selected from the same batch with close thickness in our experiment. The fresh electrode of Si shows a flat and compact surface with uniform particle distribution (Figure 6a). In comparison, the Si/C electrode before cycle presents a relatively rough surface owing to the bulk carbon matrix derived from carbonization of the lignin macromolecule at high temperatures (Figure 6b). After 100 cycles, obvious cracks and particle pulverization are found on the surface of the pure Si electrode due to the huge volume variation of the Si particle during its repeated lithiation and delithiation processes (Figure 6e). The surface of the Si/C electrode after cycling remains flat without obvious negligible cracks (Figure 6f). The Si/C composite after cycling has been investigated by high-resolution TEM (HR-TEM) and EDS mapping analysis (Figure S3). The embedding structure of the Si/C composite is maintained well after the cycling test. The corresponding element distribution of C and Si images show that the Si particles are still well encapsulated in the lignin-based carbon matrix. Therefore, the carbon matrix of the Si/C composite helps to stabilize the overall structure and suppress pulverization during cycling. In Figure 6c,d, the cross-sectional SEM images of Si and Si/C electrodes before and after 100 cycles show the changes in the thickness of both the electrodes, which more directly explain the structure stability during cycling. The thickness of the pure Si electrode increases significantly from 14 to 25 μm, while the changes in the thickness of the Si/C electrode are much smaller before and after 100 cycles (from 13 to 20 μm), indicating the great advantage of the embedding structure for the as-designed Si/C material.

4. CONCLUSIONS

In conclusion, using solar silicon waste and lignin as raw materials, a Si/C composite featuring Si particles embedded in the conducting carbon matrix is prepared by a facile solution coprecipitation process with the combination of thermal annealing. The lignin-derived hard carbon matrix effectively buffers the volume expansion/shrinkage of Si, suppresses the undesirable side reactions between electrolyte and active Si, and stabilizes the composite structure of the Si/C composite. As a result, the as-achieved Si/C electrode exhibits a high charge capacity of 706.8 mAh g^{-1} after 100 cycles and high rate capability with a capacity retention of 63.4% (based on the value at 0.2 A g^{-1}) at 2 A g^{-1}. The low cost of raw materials, facile synthesis, and superior electrochemical lithium storage properties of the Si/C composite make it promising for commercial applications in high-performance LIBs.

■ ASSOCIATED CONTENT

Supporting Information

The Supporting Information is available free of charge at https://pubs.acs.org/doi/10.1021/acsami.0c16865.

Additional experimental data including SEM, TEM, and HR-TEM images of Si–C and Si/C composite after cycles and EIS spectra of Si/C and pure Si before cycling (PDF)

■ AUTHOR INFORMATION

Corresponding Authors

Shangxian Xie – *College of Life Science and Technology, Huazhong University of Science and Technology, Wuhan 430074, China*; orcid.org/0000-0001-9448-8542; Email: shangxian_xie@hust.edu.cn

Li Wang – *Institute of Nuclear and New Energy Technology, Tsinghua University, Beijing 100084, China*; Email: wang-l@mail.tsinghua.edu.cn

Yongming Sun – *Wuhan National Laboratory for Optoelectronics, Huazhong University of Science and Technology, Wuhan 430074, China*; orcid.org/0000-0001-8528-525X; Email: yongmingsun@hust.edu.cn

Authors

Weiwei Liu – *Wuhan National Laboratory for Optoelectronics, Huazhong University of Science and Technology, Wuhan 430074, China*

Jing Liu – *Wuhan National Laboratory for Optoelectronics, Huazhong University of Science and Technology, Wuhan 430074, China*

Menghua Zhu – *Wuhan National Laboratory for Optoelectronics, Huazhong University of Science and Technology, Wuhan 430074, China*

Wenyu Wang – *Wuhan National Laboratory for Optoelectronics, Huazhong University of Science and Technology, Wuhan 430074, China*

Lei Wang – *College of Life Science and Technology, Huazhong University of Science and Technology, Wuhan 430074, China; Hubei Provincial Key Laboratory of Green Materials for Light Industry, School of Materials and Chemical Engineering, Hubei University of Technology, Wuhan 430068, China*

Xuelin Yang – *Department of Chemical and Biomolecular Engineering, China Three Gorges University, Yichang 443002, China*; orcid.org/0000-0001-5626-701X

Xiangming He – *Institute of Nuclear and New Energy Technology, Tsinghua University, Beijing 100084, China*; orcid.org/0000-0001-7146-4097

Complete contact information is available at: https://pubs.acs.org/10.1021/acsami.0c16865

Notes

The authors declare no competing financial interest.

■ ACKNOWLEDGMENTS

This work was supported by the National Key R&D Program of China (2018YFB0905400) and the Major Technological Innovation Project of Hubei Science and Technology Department (2019AAA164). Y.S. acknowledges the financial support from the Innovation Fund of Wuhan National Laboratory for Optoelectronics of Huazhong University of Science and Technology. This work is financially supported by Postdoctoral Innovative Research Post in Hubei Province, the Ministry of Science and Technology of China (No. 2019YFE0100200), and the Tsinghua University Initiative Scientific Research Program (No. 2019Z02UTY06). The authors thank the Analytical and Testing Center of Huazhong University of Science and Technology as well as the Center for Nanoscale Characterization & Devices of Wuhan National Laboratory for Optoelectronics for providing the facilities to conduct the characterization.

■ REFERENCES

(1) Breyer, C.; Bogdanov, D.; Aghahosseini, A.; Gulagi, A.; Child, M.; Oyewo, A. S.; Farfan, J.; Sadovskaia, K.; Vainikka, P. Solar Photovoltaics Demand for the Global Energy Transition in the Power Sector. *Prog. Photovoltaics Res. Appl.* **2018**, *26*, 505–523.

(2) Drouiche, N.; Cuellar, P.; Kerkar, F.; Medjahed, S.; Boutouchent-Guerfi, N.; Ould Hamou, M. Recovery of Solar Grade Silicon from Kerf Loss Slurry Waste. *Renewable Sustainable Energy Rev.* **2014**, *32*, 936–943.

(3) Zhang, L.; Zhang, L.; Zhang, J.; Hao, W.; Zheng, H. Robust Polymeric Coating Enables the Stable Operation of Silicon Micro-Plate Anodes Recovered from Photovoltaic Industry Waste for High-Performance Li-Ion Batteries. *J. Mater. Chem. A* **2015**, *3*, 15432–15443.

(4) Yoko, A.; Oshima, Y. Recovery of Silicon from Silicon Sludge Using Supercritical Water. *J. Supercrit. Fluids* **2013**, *75*, 1–5.

(5) Wang, T. Y.; Lin, Y. C.; Tai, C. Y.; Sivakumar, R.; Rai, D. K.; Lan, C. W. A novel Approach for Recycling of Kerf Loss Silicon from

Cutting Slurry Waste for Solar Cell Applications. *J. Cryst. Growth* **2008**, *310*, 3403−3406.

(6) Ye, X.; Lin, Z.; Liang, S.; Huang, X.; Qiu, X.; Qiu, Y.; Liu, X.; Xie, D.; Deng, H.; Xiong, X.; Lin, Z. Upcycling of Electroplating Sludge into Ultrafine Sn@C Nanorods with Highly Stable Lithium Storage Performance. *Nano Lett.* **2019**, *19*, 1860−1866.

(7) Yi, Z.; Wang, W.; Qian, Y.; Liu, X.; Lin, N.; Qian, Y. Mechanical Pressing Route for Scalable Preparation of Microstructured/Nanostrutured Si/Graphite cComposite for Lithium Ion Battery Anodes. *ACS Sustainable Chem. Eng.* **2018**, *6*, 14230−14238.

(8) Kim, Y. E.; Yeom, S. J.; Lee, J. E.; Kang, H.; Lee, G. H.; Kim, M. J.; Lee, S. G.; Lee, H. W.; Chae, H. G.; et al. Structural-Dependent Sodium Ion Storage Mechanism of Cellulos Nanocrystal-Based Carbon Anodes for Highly Efficient and Stable Batteries. *J. Power Sources* **2020**, *468*, 228371−228376.

(9) Feng, Z.; Chen, H.; Li, H.; Yuan, R.; Wang, F.; Chen, Z.; Zhou, B. Preparation, Characterization, and Application of Magnetic Activated Carbon for Treatment of Biologically Treated Papermaking Wastewater. *Sci. Total Environ.* **2020**, *713*, No. 136423.

(10) Zhu, H.; Luo, W.; Ciesielski, P. N.; Fang, Z.; Zhu, J. Y.; Henriksson, G.; Himmel, M. E.; Hu, L. Wood-Derived Materials for Green Electronics, Biological Devices, and Energy Applications. *Chem. Rev.* **2016**, *116*, 9305−9374.

(11) Zhang, L.; Chen, K.; Peng, L. Comparative Research about Wheat Straw Lignin from the Black Liquor after Soda-Oxygen and Soda-aq Pulping: Structural Changes and Pyrolysis Behavior. *Energy Fuels* **2017**, *31*, 10916−10923.

(12) Bajwa, D. S.; Pourhashem, G.; Ullah, A. H.; Bajwa, S. G. A Concise Review of Current Lignin Production, Applications, Products and their Environmental Impact. *Ind. Crop. Prod.* **2019**, *139*, No. 111526.

(13) Fan, P.; Mu, T.; Lou, S.; Cheng, X.; Gao, Y.; Du, C.; Zuo, P.; Ma, Y.; Yin, G. Amorphous Carbon-Encapsulated Si Nanoparticles Loading on MCMB with Sandwich Structure for Lithium Ion Batteries. *Electrochim. Acta* **2019**, *306*, 590−598.

(14) Cui, Y.; Wan, J.; Ye, Y.; Liu, K.; Chou, L. Y.; Cui, Y. A Fireproof, Lightweight, Polymer-Polymer Solid-State Electrolyte for Safe Lithium Batteries. *Nano Lett.* **2020**, *20*, 1686−1692.

(15) Zhu, G.; Jiang, W.; Yang, J. Engineering Carbon Distribution in Silicon-based Anodes at Multiple Scales. *Chem. - Eur. J.* **2020**, *26*, 1488−1496.

(16) Wang, J.; Liao, L.; Lee, H. R.; Shi, F.; Huang, W.; Zhao, J.; Pei, A.; Tang, J.; Zheng, X.; Chen, W.; Cui, Y. Surface-Engineered Mesoporous Silicon Microparticles as High-Coulombic-Efficiency Anodes for Lithium-Ion Batteries. *Nano Energy* **2019**, *61*, 404−410.

(17) Sun, Y.; Liu, N.; Cui, Y. Promises and Challenges of Nanomaterials for Lithium-based Rechargeable Batteries. *Nat. Energy* **2016**, *1*, No. 16071.

(18) Li, G.; Li, J. Y.; Yue, F.-S.; Xu, Q.; Zuo, T. T.; Yin, Y. X.; Guo, Y. G. Reducing the Volume Deformation of High Capacity SiO_x/G/C Anode toward Industrial Application in High Energy Density Lithium-Ion Batteries. *Nano Energy* **2019**, *60*, 485−492.

(19) Jeong, Y. K.; Choi, J. W. Mussel-Inspired Self-Healing Metallopolymers for Silicon Nanoparticle Anodes. *ACS Nano* **2019**, *13*, 8364−8373.

(20) Shao, R.; Niu, J.; Zhu, F.; Dou, M.; Zhang, Z.; Wang, F. A Facile and Versatile Strategy towards High-Performance Si Anodes for Li-Ion Capacitors: Concomitant Conductive Network Construction and Dual-Interfacial Engineering. *Nano Energy* **2019**, *63*, No. 103824.

(21) Choi, S.; Kwon, T.-W.; Coskun, A.; Choi, J. W. Highly Elastic Binders Integrating Polyrotaxanes for Silicon Microparticle Anodes in Lithium Ion Batteries. *Science* **2017**, *357*, 279.

(22) Cho, Y.; Kim, J.; Elabd, A.; Choi, S.; Park, K.; Kwon, T.-w.; Lee, J.; Char, K.; Coskun, A.; Choi, J. W. A Pyrene−Poly(acrylic Acid)-Polyrotaxane Supramolecular Binder Network for High-Performance Silicon Negative Electrodes. *Adv. Mater.* **2019**, *31*, No. 1905048.

(23) Yeom, S. J.; Lee, C.; Kang, S.; Wi, T. U.; Lee, C.; Chae, S.; Cho, J.; Shin, D. O.; Ryu, J.; Lee, H. W. Native Void Space for Maximum Volumetric Capacity in Silicon-based Anodes. *Nano Lett.* **2019**, *19*, 8793−8800.

(24) Chae, S.; Choi, S. H.; Kim, N.; Sung, J.; Cho, J. Integration of Graphite and Silicon Anodes for the Commercialization of High-Energy Lithium-Ion Batteries. *Angew. Chem., Int. Ed.* **2019**, *58*, 2−28.

(25) Yi, Z.; Lin, N.; Xu, T.; Qian, Y. TiO_2 Coated Si/C Interconnected Microsphere with Stable Framework and Interface for High-Rate Lithium Storage. *Chem. Eng. J.* **2018**, *347*, 214−222.

(26) Chen, J.; Fan, X.; Li, Q.; Yang, H.; Khoshi, M. R.; Xu, Y.; Hwang, S.; Chen, L.; Ji, X.; Yang, C.; He, H.; Wang, C.; Garfunkel, E.; Su, D.; Borodin, O.; Wang, C. Electrolyte Design for LiF-rich Solid-Electrolyte Interfaces to Enable High-Performance Microsized Alloy Anodes for Batteries. *Nature Energy* **2020**, *5*, 386−397.

(27) Shen, C.; Fang, X.; Ge, M.; Zhang, A.; Liu, Y.; Ma, Y.; Mecklenburg, M.; Nie, X.; Zhou, C. Hierarchical Carbon-Coated bBall-Milled Silicon: Synthesis and Applications in Free-Standing Electrodes and High-Voltage Full Lithium-Ion Batteries. *ACS Nano* **2018**, *12*, 6280−6291.

(28) Zhang, H.; Zong, P.; Chen, M.; Jin, H.; Bai, Y.; Li, S.; Ma, F.; Xu, H.; Lian, K. In Situ Synthesis of Multilayer Carbon Matrix Decorated with Copper Particles: Enhancing the Performance of Si as Anode for Li-Ion Batteries. *ACS Nano* **2019**, *13*, 3054−3062.

(29) Zhang, R.; Du, Q.; Wang, L.; Zheng, Z.; Guo, L.; Zhang, X.; Yang, X.; Yu, H. Unlocking the Response of Lignin Structure for Improved Carbon Fiber Production and Mechanical Strength. *Green Chem.* **2019**, *21*, 4981−4987.

(30) Jin, Y.; Zhu, B.; Lu, Z.; Liu, N.; Zhu, J. Challenges and Recent Progress in the Development of Si Anodes for Lithium-Ion battery. *Adv. Energy Mater.* **2017**, *7*, No. 1700715.

(31) Chen, C.; Jin, D.; Ouyang, X.; Zhao, L.; Qiu, X.; Wang, F. Effect of Structural Characteristics on the Depolymerization of Lignin into Phenolic Monomers. *Fuel* **2018**, *223*, 366−372.

(32) Duan, D.; Ruan, R.; Wang, Y.; Liu, Y.; Dai, L.; Zhao, Y.; Zhou, Y.; Wu, Q. Microwave-Assisted Acid Pretreatment of Alkali Lignin: Effect on Characteristics and Pyrolysis Behavior. *Bioresour. Technol.* **2018**, *251*, 57−62.

(33) Lu, B.; Ma, B.; Deng, X.; Li, W.; Wu, Z.; Shu, H.; Wang, X. Cornlike Ordered Mesoporous Silicon Particles Modified by Nitrogen-Doped Carbon Layer for the Application of Li-Ion Battery. *ACS Appl. Mater. Interfaces* **2017**, *9*, 32829−32839.

(34) Yi, Z.; Qian, Y.; Cao, C.; Lin, N.; Qian, Y. Porous Si/C Microspheres Decorated with Stable Outer Carbon Interphase and Inner Interpenetrated Si@C Channels for Enhanced Lithium Storage. *Carbon* **2019**, *149*, 664−671.

(35) Yan, Y.; Xu, Z.; Liu, C.; Dou, H.; Wei, J.; Zhao, X.; Ma, J.; Dong, Q.; Xu, H.; He, Y. S.; Ma, Z. F.; Yang, X. Rational Design of the Robust Janus Shell on Silicon Anodes for High-Performance Lithium-Ion Batteries. *ACS Appl. Mater. Interfaces* **2019**, *11*, 17375−17383.

(36) Xu, Q.; Sun, J. K.; Yu, Z. L.; Yin, Y. X.; Xin, S.; Yu, S. H.; Guo, Y. G. SiO_x Encapsulated in Graphene Bubble Film: An Ultrastable Li-Ion Battery Anode. *Adv Mater.* **2018**, *30*, No. 1707430.

(37) Luo, W.; Wang, Y.; Wang, L.; Jiang, W.; Chou, S.-L.; Dou, S. X.; Liu, H. K.; Yang, J. Silicon/Mesoporous Carbon/Crystalline TiO_2 Nanoparticles for Highly Stable Lithium Storage. *ACS Nano* **2016**, *10*, 10524−10532.

(38) Stevens, D. A.; Dahn, J. R. The Mechanisms of Lithium and Sodium Insertion in Carbon Materials. *J. Electrochem. Soc.* **2001**, *148*, A803−811.

(39) Buiel, E.; Dahn, J. R. Li-Insertion in Hard Carbon Anode Materials for Li-Ion Batteries. *Electrochim. Acta* **1999**, *45*, 121−130.

(40) Liu, H.; Shan, Z.; Huang, W.; Wang, D.; Lin, Z.; Cao, Z.; Chen, P.; Meng, S.; Chen, L. Self-Assembly of Silicon@Oxidized Mesocarbon Microbeads Encapsulated in Carbon as Anode Material for Lithium-Ion Batteries. *ACS Appl. Mater. Interfaces* **2018**, *10*, 4715−4725.

(41) Sun, A.; Zhong, H.; Zhou, X.; Tang, J.; Jia, M.; Cheng, F.; Wang, Q.; Yang, J. Scalable Synthesis of Carbon-Encapsulated Nano-

Si on Graphite Anode Material with High Cyclic Stability for Lithium-Ion Batteries. *Appl. Surf. Sci.* **2019**, *470*, 454−461.

(42) Liu, Z.; Zhao, Y.; He, R.; Luo, W.; Meng, J.; Yu, Q.; Zhao, D.; Zhou, L.; Mai, L. Yolk@Shell SiO/C Microspheres with Semi-Graphitic Carbon Coating on the Exterior and Interior Surfaces for Durable Lithium Storage. *Energy Storage Mater.* **2019**, *19*, 299−305.

(43) Li, D.; Müller, M. B.; Gilje, S.; Kaner, R. B.; Wallace, G. G. Processable Aqueous Dispersions of Graphene Nanosheets. *Nat. Nanotechnol.* **2008**, *3*, 101−105.

(44) Jin, Y.; Zhang, S.; Zhu, B.; Tan, Y.; Hu, X.; Zong, L.; Zhu, J. Simultaneous Purification and Perforation of Low-Grade Si Sources for Lithium-Ion Battery Anode. *Nano Lett.* **2015**, *15*, 7742−7747.

(45) Hwang, T. H.; Lee, Y. M.; Kong, B. S.; Seo, J. S.; Choi, J. W. Electrospun Core-Shell Fibers for Robust Silicon Nanoparticle-based Lithium Ion Battery Anodes. *Nano Lett.* **2012**, *12*, 802−807.

(46) Lou, S.; Cheng, X.; Gao, J.; Li, Q.; Wang, L.; Cao, Y.; Ma, Y.; Zuo, P.; Gao, Y.; Du, C.; Huo, H.; Yin, G. Pseudocapacitive Li^+ Intercalation in Porous $Ti_2Nb_{10}O_{29}$ Nanospheres Enables Ultra-Fast Lithium Storage. *Energy Storage Mater.* **2018**, *11*, 57−66.

(47) Xu, Q.; Li, J. Y.; Sun, J. K.; Yin, Y. X.; Wan, L. J.; Guo, Y. G. Watermelon-Inspired Si/C Microspheres with Hierarchical Buffer Structures for Densely Compacted Lithium-Ion Battery Anodes. *Adv. Energy Mater.* **2017**, *7*, No. 1601481.

(48) Liu, W.; Zhu, M.; Liu, J.; Li, X.; Liu, J. Flexible Aasymmetric Supercapacitor with High Energy Density based on Optimized MnO_2 Cathode and Fe_2O_3 Anode. *Chin. Chem. Lett.* **2019**, *30*, 750−756.

(49) Wu, F.; Wang, H.; Shi, J.; Yan, Z.; Song, S.; Peng, B.; Zhang, X.; Xiang, Y. Surface Modification of Silicon Nanoparticles by an "Ink" Layer for Advanced Lithium Ion Batteries. *ACS Appl. Mater. Interfaces* **2018**, *10*, 19639−19648.

(50) Wei, L.; Hou, Z.; Wei, H. Porous Sandwiched Graphene/Silicon Anodes for Lithium Storage. *Electrochim. Acta* **2017**, *229*, 445−451.

(51) Kwon, H. J.; Hwang, J. Y.; Shin, H. J.; Jeong, M. G.; Chung, K. Y.; Sun, Y. K.; Jung, H. G. Nano/Microstructured Silicon-Carbon Hybrid Composite Particles Fabricated with Corn Starch Biowasted as Anode Materials for Li-Ion Batteries. *Nano Lett.* **2020**, *20*, 625−635.

(52) Zhang, C. C.; Cai, X.; Chen, W. Y.; Yang, S. Y.; Xu, D. H.; Fang, Y. P.; Yu, X. Y. 3D Porous Silicon/n-Doped Carbon Composite Derived from Bamboo Charcoal as High-Performance Anode Material for Lithium-Ion Batteries. *ACS Sustainable Chem. Eng.* **2018**, *6*, 9930−9939.

(53) Liu, J.; Kopold, P.; Aken, P. A.; Maier, J.; Yu, Y. Energy Storage Materials from Nature through Nanotechnology: A Sustainable Route from Reed Plants to a Silicon Anode for Lithium-Ion Batteries. *Angew. Chem.* **2015**, *127*, 9768−9772.

(54) China Photovoltaic Industry Association, Development of Polysilicon Industry. 2020, https://www.sohu.com/a/401165611_418320. (accessed Aug 20, 2020).